RSC Advances

ROYAL SOCIETY OF CHEMISTRY

www.rsc.org/advances

Synthesis and near-infrared luminescence of $La_3GaGe_5O_{16}:Cr^{3+}$ phosphors

Jun Zhou[1], Zhiguo Xia[1,2*]

[1]*School of Materials Sciences and Technology, China University of Geosciences, Beijing 100083, China*

[2]*School of Materials Sciences and Engineering, University of Science and Technology Beijing, Beijing 100083, China*

---

[*] **Corresponding author:**

Zhiguo Xia

E-mail: **xiazg@ustb.edu.cn**

School of Materials Sciences and Engineering, University of Science and Technology Beijing, Beijing 100083, China

Tel. : +86-10-8237-7955;

Fax. : +86-10-8237-7955

Abstract: A novel Cr^{3+}-doped $La_3GaGe_5O_{16}$ phosphor was synthesized by a solid-state reaction, and the phase formation and microstructure, near-infrared (NIR) photoluminescence (PL) properties and PL thermal stability were investigated in detail. The excitation spectrum of $La_3GaGe_5O_{16}:Cr^{3+}$ at 270, 415 and 573nm corresponded to three spin-allowed Cr^{3+} d-d intra-transitions of $^4A_2$-$^4T_1$ (^4P), $^4A_2$-$^4T_1$ (^4F), and $^4A_2$-$^4T_2$ (^4F), respectively, among which the main red emission peak observed at 700 nm is identified, which is due to ^2E-$^4A_2$ transition from Cr^{3+} ions. It is further proved that the dipole-diople interactions results in the concentration quenching of Cr^{3+} in $La_3GaGe_5O_{16}:Cr^{3+}$ phosphors, and the energy-transfer distance at quenching concentration was around 26.90 Å. Moreover, thermal quenching luminescence results reveal that $La_3GaGe_5O_{16}:Cr^{3+}$ exhibits good thermal stability. The above results indicate that $La_3GaGe_5O_{16}:Cr^{3+}$ has potential practical applications in luminescent solar concentrator with broad-band absorption.

1. Introduction

Recently, solar cells have attracted much attention because they are promising devices for inexpensive and large-scale solar energy conversion. However, the efficiency in the commercial Si solar cells is just 15%, which means that most of sunlight energy is lost.[1] One of the main energy loss in the conversion of solar energy to electricity is attributed to the so-called spectral mismatch between incident solar photon energies and the energy gap (E_g) of the cells.[2] As we know, the main energy of the solar emission dispersed on the earth surface is in visible light region, but E_g of the Si cell is suitable to the absorption in far-red and near-infrared regions. Consequently, luminescent solar concentrator (LSC) was developed that can collect solar photons and transfer them to the photons matching E_g of the Si solar cells. Moreover, when luminescent materials with efficient UV-Vis absorption and deep-red and near-infrared emissions are applied in LSCs, the efficiency of Si cells would be significantly enhanced.[3] Therefore, studies on new phosphors with deep-red and near-infrared emissions are highly desirable.

Interest in Cr^{3+} activated inorganic materials is widespread because of its deep red colors and bright photoluminescence. Cr^{3+} is the most stable state of chromium element because of its narrow-band emissions (usually near 700 nm) due to the spin-forbidden ^2E-$^4A_2$ transition, or a broadband emission (650-1600 nm) due to the spin-allowed $^4T_2$-$^4A_2$ transition, which strongly depends on the crystal-field environment of the host lattices.[4-6] Therefore Cr^{3+} can be used as a luminescent dopant with red emission in LSCs. This dopant also has its specific use in modern

technologies, for example, tunable solid-state lasers, high temperature sensors, and high-pressure calibrants.[7-9] Recently, various Cr^{3+} doped host materials has been widely investigated by several research groups and its emission in various compounds like $Y_3Al_5O_{12}$,[10] $MgAl_2O_4$,[11] $Cs_2NaScCl_6$[12] and many others have also been studied.

As for the development of Cr^{3+}-activated optical materials with tunable red and NIR emission, gallogermanates were usually used as the host materials since Cr^{3+} ions can substitute for Ga^{3+} ions in distorted octahedral sites. Moreover, suitable host crystal-field strength around Cr^{3+} will help to achieve intense deep red emission.[13] As we know, the reported Cr^{3+}-doped gallogermanates include $M_3Ga_2Ge_4O_{14}:Cr^{3+}$ (M = Sr or Ca),[14] $La_3Ga_5GeO_{14}:Cr^{3+}$,[13] and $Zn_3Ga_2Ge_2O_{10}:Cr^{3+}$.[5] In 1998, G. Adiwidjaja firstly reported the new gallogermanate of lanthanum compound, $La_3GaGe_5O_{16}$, as a single crystal form and revealed its chemical composition and detailed crystal structure.[15] However, to the best of our knowledge, there are no further reports on this compound and their potential application as optical materials hosts except for our recent work.[16] In this paper, we have found that Cr^{3+}-doped lanthanide gallogermanate garnet ($La_3GaGe_5O_{16}:Cr^{3+}$) phosphors fabricated by a solid-state reaction method can exhibit remarkable red emission peak at 700 nm. And the energy transfer mechanism, photoluminescence decay curves and the temperature dependent PL behaviour have also been investigated.

2. Experimental

2.1 Materials and synthesis

A series of rare earth-doped $La_3Ga_{1-x}Ge_5O_{16}$:xCr^{3+} phosphors were synthesized by s high temperature solid-state reaction. The starting materials were analytical reagent grade La_2O_3 (99.995%), Ga_2O_3 (99.9%), GeO_2 (99.9%) and Cr_2O_3 (99.9%). Firstly, the starting materials were thoroughly mixed in an agate mortar according to the given stoichiometric amounts. Then, the mixture was put into an alumina crucible and calcined in a muffle furnace at 1250 °C for 5 h in air. After the samples were cooled to room temperature, the phosphors were finally obtained.

2.2 Characterization methods

The phase structures of the as-prepared samples were carried out on a SHIMADZU model XRD-6000 diffractometer using Cu Kα radiation (λ = 0.15406 nm) at 40 kV and 30 mA. Microstructure observation was observed using a scanning electron microscopy (SEM) (HITACHI, S-3400). Room temperature excitation and emission spectra were measured on a fluorescence spectrophotometer (F-4600, HITACHI, Japan) with a photomultiplier tube operating at 400 V, and a 150 W Xe lamp used as the excitation lamp. The temperature-dependence luminescence properties were measured on the same spectrophotometer, which was combined with a self-made heating attachment and a computer-controlled electric furnace. The decay curves were recorded on a spectrofluorometer (HORIBA, JOBIN YVON FL3-21), and the 460 nm pulse laser radiation (nano-LED) was used as the excitation source.

3. Results and discussion

3.1 Phase formation and microstructure

The diffraction pattern is usually used to identify the crystal structure and the phase purity of the sample. Fig. 1(a) shows the XRD patterns of as-prepared $La_3GaGe_5O_{16}$, $La_3Ga_{0.97}Ge_5O_{16}$:0.03Cr^{3+} and $La_3Ga_{0.85}Ge_5O_{16}$:0.15Cr^{3+} phosphors. From Fig. 1(a), we can know that all of the diffraction peaks are in good agreement with the reported triclinic phase of $La_3GaGe_5O_{16}$ (JCPDS 89-0211) and no detectable impurity phase is observed, which indicates that single-phased $La_3GaGe_5O_{16}$ powder can be obtained by the solid-state method. Furthermore, based on the consideration of the similar effective ionic radius and valence of cations, Cr^{3+} ions prefer to occupy the Ga^{3+} sites in the host. SEM image of the selected $La_3Ga_{0.97}Ge_5O_{16}$:0.03Cr^{3+} phosphor is presented in Fig. 1(b), from which the phosphor particles were well dispersed, and their mean size was about 3-8 μm, and the uniform distribution and small particles verified that the as-prepared phosphors can be potential in the future application.

3.2 Luminescence properties and the corresponding mechanism

Cr^{3+} belong to $3d^3$ electronic configurations and the splitting of the energy levels in octahedral symmetry can be expressed by well-known Tanabe-Sugano energy level diagram as shown in Fig. 2(a). The d^3 configuration gives rise to two quartet terms and ^4F and ^4P with ^4F term lying lower to ^4P as per Hund's rule. In addition to these quartet terms, there are several doublet terms. The ^2G term splits into ^2E level, and the $^4A_2$, $^4T_2$, and $^4T_1$ levels come from the 4F term.[17-18] Moreover, the luminescence and excitation spectra depend on the relative positions between $^4T_2$ and ^2E levels, which is

shown in Fig. 2(b) as a configurational coordinate diagram. When Cr^{3+} ions locate in the intermediate field sites, $^4T_2$ is above the ^2E level, resulting in the R lines emission (assigned to ^2E-$^4A_2$ transition). And when Cr^{3+} ions locate in the weak field sites, $^4T_2$ is under the ^2E level, which causes the band emission (assigned to $^4T_2$-$^4A_2$ transition). Therefore, Fig. 3 shows the normalized excitation and emission spectra of $La_3Ga_{0.97}Ge_5O_{16}$:0.03Cr^{3+} at room temperature, which can be used to understand the corresponding transitions of Cr^{3+}. Accordingly, Fig. 4 shows schematic energy levels of Cr^{3+}, the corresponding excitation spectrum and electron transitions for the Cr^{3+}-doped $La_3GaGe_5O_{16}$ phosphor is also given based on the measurement results in Fig. 3. It is found that, under excitation at 415 nm, Cr^{3+}-doped $La_3GaGe_5O_{16}$ phosphor exhibits a broadening ^2E-$^4A_2$ emission peaking at 700 nm that superimposes on a broad emission band extending from 600 to 900 nm. The broadening of the ^2E-$^4A_2$ emission is probably caused by the electron-phonon coupling because the phonon energy of the Cr^{3+} dopant matches well with that of the gallate-containing host,[19] whereas the broadband emission may be ascribed to the $^4T_2$-$^4A_2$ transitions from some disordered Cr^{3+} ions in the gallogermanate system.[20] The excitation spectrum monitored at 700 nm covers a very broad spectral region (from 200 to 650 nm) consists of three main excitation bands originating from the inner transitions of Cr^{3+}, including the 270 nm band originating from the $^4A_2$-$^4T_1$ (^4P) transition, the 415 nm band originating from the $^4A_2$-$^4T_1$ (^4F) transition and 573 nm band originating from the $^4A_2$-$^4T_2$ (^4F) transition.[21] Based on the above PLE spectrum for $La_3Ga_{0.97}Ge_5O_{16}$:0.03Cr^{3+}, it proves that the obtained sample has excellent n-UV and

visible excitation properties, which in turn means that this kind of phosphor has the potential as a promising NIR-emitting phosphor system for LSCs with broad-band absorption.

Fig. 5 presents the emission (λ_{ex} = 415 nm) spectra of the $La_3Ga_{1-x}Ge_5O_{16}$:xCr^{3+} phosphors with different concentrations of Cr^{3+} (ranging from 0.01 to 0.15) at room temperature. As is shown in Fig. 5, this series of samples all produce a strong and broad-band NIR emission with a peak at around 700 nm, and the emission spectra have no obvious changes in the spectral configuration except for the emission intensity. Furthermore, the inset shows the Cr^{3+} content dependent PL intensities, and Cr^{3+} concentration (x) in $La_3Ga_{1-x}Ge_5O_{16}$:xCr^{3+} reaches a saturation point at x = 0.03. After that, the PL intensity begins to decrease with increasing Cr^{3+} concentration due to the concentration quenching effect.

It is accepted that energy quenching can be ascribed on the energy transfer between Cr^{3+} ions followed by energy transfer to traps or quenching sites. Therefore, in order to further confirm the process of energy transfer between Cr^{3+} ions in the $La_3GaGe_5O_{16}$:Cr^{3+} phosphor, the interaction type between sensitizers or between the sensitizer and activator can be calculated by the following equation:[22]

$$\frac{I}{x} = K\left[1+\beta\left(x\right)^{\frac{\theta}{3}}\right]^{-1} \quad (1)$$

In this equation x is the activator concentration which is not less than the critical concentration, I/x is the emission intensity (I) per activator concentration (x), K and β are constants for the same excitation condition for a given host crystal, and θ is an indication of electric multipolar character. It is previously reported that θ = 3 for the

energy transfer among the nearest-neighbor ions, as θ = 6, 8 and 10 corresponds to dipole-dipole (*d*-*d*), dipole-quadrupole (*d*-*q*), and quadrupole-quadrupole (*q*-*q*) interactions, respectively. To get a correct θ value, the dependence of lg(*I*/*x*) on lg(*x*) is plotted, and it yield a straight line with a slope equal to $-\theta/3$. As shown in Fig. 6, the slope is -1.93. The value of θ can be calculated as 5.79, which is close to 6 that means the quenching is dipole-dipole interactions in $La_3GaGe_5O_{16}:Cr^{3+}$ phosphors.

The critical distance of energy transfer R_c was calculated by using the concentration quenching method. R_c can be calculated using the relation given by Blasse:[23]

$$R_c \approx 2\left(\frac{3V}{4\pi x_c N}\right)^{\frac{1}{3}} \quad (2)$$

here N is the number of molecules in the unit cell, V is the unit cell volume and x_c is the critical concentration. For $La_3GaGe_5O_{16}$ host, the crystallographic parameters are N = 2, V = 611.81 Å^3 and x_c is 0.03. According to the above equation, the critical distance of energy transfer is estimated to be about 26.90 Å.

In order to further understand the concentration quenching in detail, the decay curves for the $La_3Ga_{1-x}Ge_5O_{16}:xCr^{3+}$ (x = 0.01, 0.03, 0.05, 0.08 and 0.15) phosphors excited at 460 nm and monitored at 700 nm are measured and depicted in Fig. 7. As shown in Fig. 7, it is found that the decay curves are well fitted with a second order exponential equation:[24]

$$I(t) = A_1 \exp(-t/\tau_1) + A_2 \exp(-t/\tau_2) \quad (3)$$

Where, I is the luminescence intensity, A_1 and A_2 are constants, t is the time, τ_1 and τ_2 are rapid and slow lifetime values for exponential components, respectively. Based on

the Eq. (3), and we can obtain the A_1, A_2, τ_1 and τ_2 values based on the fitting of the decay curves. Therefore, the effective lifetime constant (τ^*) can be calculated as:[25]

$$\tau^* = \left(A_1\tau_1^{\ 2} + A_2\tau_2^{\ 2}\right)/\left(A_1\tau_1 + A_2\tau_2\right) \quad (4)$$

The effective decay time (τ^*) were calculated to be 75.19, 69.66, 60.18, 47.65 and 40.29 μs for $La_3Ga_{1-x}Ge_5O_{16}$:xCr^{3+} with x = 0.01, 0.03, 0.05, 0.08 and 0.15, respectively. The obtained result shows that the measured lifetime τ of Cr^{3+} emission decreases faster with higher doping Cr^{3+} concentration. The measured lifetime is also related to the total relaxation rate by:[26-27]

$$\frac{1}{\tau} = \frac{1}{\tau_0} + A_{\mathrm{nr}} + P_t \quad (5)$$

Where τ_0 is the radiative lifetime, A_{nr} is the nonradiative rate due to multiphonon relaxation, P_t is the energy transfer rate between Cr^{3+} ions, and τ is equivalent to τ^*. With increasing Cr^{3+} concentration, the distance between Cr^{3+} ions decreases. Therefore, both the energy transfer rate between Cr^{3+}- Cr^{3+} and the probability of energy transfer to luminescent killer sites increased. Consequently, the lifetimes are shortened as increasing Cr^{3+} concentration.[28]

3.3 Thermal stability behavior

The thermal stability of phosphor is one of important parameters for the possible application. Fig. 8 shows the dependence of PL spectra of $La_3Ga_{0.99}Ge_5O_{16}$:$0.01Cr^{3+}$, $La_3Ga_{0.97}Ge_5O_{16}$:$0.03Cr^{3+}$ and $La_3Ga_{0.85}Ge_5O_{16}$:$0.15Cr^{3+}$ on temperature excited by 415 nm light. The relative emission intensities of all phosphors decrease with increasing temperature in the range of 25 °C to 300 °C. We observed a decay of 12.9% for $La_3Ga_{0.99}Ge_5O_{16}$:$0.01Cr^{3+}$, 20.5% for $La_3Ga_{0.97}Ge_5O_{16}$:$0.03Cr^{3+}$, and 32.6% for

$La_3Ga_{0.85}Ge_5O_{16}$:0.15Cr^{3+} at 100 °C. The thermal quenching of emission intensity can be explained by several mechanisms. A widely accepted mechanism is the electronic transition through the intersection between the ground and excited states. In other words this mechanism is described as a large displacement between the ground and excited state in the configuration coordinate diagram.[29] Moreover, the full-width at half-maximum (FWHM) of the PL spectra of all phosphors increases with increasing temperature, which can be described by using the Boltzmann distribution according to the following equation:[30]

$$FWHM(T) = W_0\sqrt{\coth\left(\frac{\mathrm{hw}}{2\mathrm{kT}}\right)} \quad (6)$$

$$W_0 = \sqrt{8\ln 2}(hw)\sqrt{S} \quad (7)$$

Where W_0 is the FWHM at 0K, hw is the energy of the lattice vibration that interacts with the electronic transitions, S is the Huang-Rhys-Pekar parameter, and k is the Boltzmann constant. With the increasing of temperature, the bond length between luminescence center and its coordinated ions increase which cripple the intensity of crystal field and the interaction between electron and phonon play as the leading role, consequently the FWHM of the emission line is broadened.

To better understand the temperature dependence of photoluminescence, the activation energy was calculated using the Arrhenius equation:[31-32]

$$I_T = \frac{I_0}{1 + c\exp(-\frac{\Delta E}{kT})} \quad (8)$$

where I_0 is the initial PL intensity of the phosphor at room temperature, I_T is the PL intensity at different temperatures, c is a constant, ΔE is the activation energy for thermal quenching, and k is Boltzmann constant (8.62 $\times 10^{-5}$ eV). According to the equation, the plot of $\ln[(I_0/I_T)-1]$ *vs.* $1/k$T yields a straight line, and the activation

energy ΔE is obtained from the slop of the plot. As shown in Fig. 9, ΔE is calculated to be 0.309, 0.236 and 0.234 eV for the $La_3Ga_{0.99}Ge_5O_{16}:0.01Cr^{3+}$, $La_3Ga_{0.97}Ge_5O_{16}:0.03Cr^{3+}$ and $La_3Ga_{0.85}Ge_5O_{16}:0.15Cr^{3+}$ phosphors, respectively. From the results, we can find that the samples with low Cr^{3+} concentration has larger ΔE values corresponding to better thermal stability properties, which means that the sample with high Cr^{3+} concentration possible possess more de-activation channels originating from the enhanced interaction among the increasing Cr^{3+} ions.

4. Conclusion

In summary, a novel near-infrared (NIR) phosphor, $La_3GaGe_5O_{16}:Cr^{3+}$ was synthesized via the solid-state reaction. The $La_3GaGe_5O_{16}:Cr^{3+}$ phosphor exhibited NIR emission peaked at 700 nm under the excitation of 415 nm UV radiation. The optimal doping concentration of Cr^{3+} is 3 mol%, and the concentration quenching mechanism is determined to be dipole-dipole interaction. Moreover, the temperature dependence of luminescence shows that the thermal quenching behavior is related to the Cr^{3+} doping concentration and the emission intensity of Cr^{3+} decrease with the increase of temperature and Cr^{3+} will decay faster with higher doping concentration. Preliminary studies showed that $La_3GaGe_5O_{16}:Cr^{3+}$ has potential practical applications in luminescent solar concentrator with broad-band absorption and emission.

Acknowledgements

The present work was supported by the National Natural Science Foundations of China

(Grant No. No.51002146, No.51272242), Natural Science Foundations of Beijing (2132050), the Program for New Century Excellent Talents in University of Ministry of Education of China (NCET-12-0950), Beijing Nova Program (Z131103000413047), Beijing Youth Excellent Talent Program (YETP0635) and the Funds of the State Key Laboratory of New Ceramics and Fine Processing, Tsinghua University (KF201306)

References

1 D. Timmerman, I. Izeddin, P. Stallinga, I. N. Yassievich and T. Gregorkiewicz, *Nat. Photonics.,* 2008, **2**, 105.

2 B. S. Richards, *Sol. Cells.,* 2006, **90**, 2329.

3 L. M. Shao and X. P. Jing, *J. Lumin.,* 2011, **131**, 1216.

4 B. Qiao, Z. L. Tang, Z. T. Zhang and L. Chen, *Mater. Lett.,* 2007, **61**, 401.

5 Z. W. Pan, Y. Y. Lu and F. Liu, *Nat. Mater.,* 2012, **11**, 58.

6 Y. Li, S. F. Zhou, Y. Y. Li, K. Sharafudeen, Z. J. Ma, G. P. Dong, M. Y. Peng and J. R. Qiu, *J. Mater. Chem. C,* 2014, **2**, 2657.

7 V. Singh, R. P. S. Chakradhar, J. L. Rao and J. J. Zhu, *Mater. Chem. Phys.,* 2008, **111**, 143.

8 P. R. Wamsley and K. L. Bray, *J. Lumin.,* 1994, **59**, 11.

9 K. T. V. Grattan, R. K. Selli and A. W. Palmer, *Rev. Sci. Instrum.,* 1988, **59**, 1328.

10 S. M. Kaczmarek. W. Chen and G. Boulon, *Cryst. Res. Technol.,* 2006, **41**, 41.

11 V. Singh, R. P. S. Chakradhar, J. L. Rao and D. K. Kim, *J. Lumin.,* 2009, **129**, 130.

12 O. S. Wenger, R. Valiente and H. U. Gudel, *J. Chem. Phys.,* 2001, **115**, 3819.

13 W. Z. Yan, F. Liu, Y. Y. Lu, X. J. Wang, M. Yin and Z. W. Pan, *Opt. Express,* 2010, **18**, 20215.

154 P. I. Macfarlane, T. P. J. Han, B. Henderson and A. A. Kaminskii, *Opt. Mater.,* 1994, **3**, 15.

15 G. Adiwidjaja, M. Broker, C. Claus, K. Friese, K. H. Klaska, O. Jarchow, M. Ruks and I. Wozniak, *Z. Kristallogr.,* 1998, **213**, 223.

16 J. Zhou and Z. G. Xia, *J. Mater. Chem. C*, 2014, **2**, 6978.

17 M. N. Sanz-Ortiz, F. Rodríguez, I. Hernández, R. Valiente and S. Kück, *Phys. Rev. B,* 2010, **81**, 045114.

18 I. Hernández, F. Rodríguez and A. Tressaud, *Inorg. Chem.,* 2008, **47**, 10288.

19 P. D. Rack, J. J. Peterson, M. D. Potter and W. J. Park, *J. Mater. Res.,* 2001, **16**, 1429.

20 M. Grinberg, *Opt. Mater.,* 2002, **9**, 37.

21 I. M. Peter, H. Brian, H. Keith and G. Marek, *J. Phys. Condens. Matter.,* 1996, **8**, 3933.

22 G. Blasse, *Phys. Lett.,* 1968, **28**, 444.

23 G. Blasse, *J. Solid State Chem.,* 1986, **62**, 207.

24 C. H. Huang and T. M. Chen, *J. Phys. Chem. C,* 2011, **115**, 2349.

25 S. Murakami, M. Herren, D. Rau and M. Morita, *Inorg. Chim. Acta.,* 2000, **300**, 1014.

26 B. Henderson and G. F. Imbusch, *Optical Spectroscopy of Inorganic Solids,* Clarendon, Oxford, 1989, p, 151.

27 D. Wang and N. Kodama, *J. Solid State Chem.,* 2009, **182**, 2219.

28 D. Y. Wang, C. H. Huang, Y. C. Wu and T. M. Chen, *J. Mater. Chem.,* 2011, **21**, 10818.

29 G. H. Munoz, C. L. de la Cruz, A. F. Munoz and J. O. Rubio, *J. Mater. Sci. Lett.,* 1988, **7**, 1310.

30 P. Dorenbos, *J. Lumin*., 2003, **104**, 239.

21 Z. G. Xia, R. S. Liu, K. W. Huang and V. Droid, *J. Mater. Chem.,* 2012, **22**, 15183.

32 J. Zhou, Z. G. Xia, M. X. Yang and K. Shen, *J. Mater. Chem.,* 2012, **22**, 21935.

The figure captions are as follows,

Fig. 1 (a) XRD patterns of as-prepared $La_3GaGe_5O_{16}$, $La_3Ga_{0.97}Ge_5O_{16}$:0.03Cr^{3+}, and $La_3Ga_{0.85}Ge_5O_{16}$:0.15Cr^{3+} phosphors, the standard data for $La_3GaGe_5O_{16}$ (JCPDS card no. 89-0211) is shown as a reference. (b) SEM image of the selected $La_3Ga_{0.97}Ge_5O_{16}$:0.03Cr^{3+} phosphor.

Fig. 2 (a) Tunabe-sugnano diagram for Cr^{3+} in $La_3Ga_{0.97}Ge_5O_{16}$. (b) Mechanistic configurational coordinate diagram illustrating different emission channels. The solid and dashed arrows represent the emissions from the Cr^{3+} ions located in the intermediate and weak field sites, respectively.

Fig. 3 Normalized excitation and emission spectra of $La_3Ga_{0.97}Ge_5O_{16}$:0.03Cr^{3+} phosphor at room temperature.

Fig. 4 Schematic energy levels of Cr^{3+}, the corresponding excitation spectrum and electron transitions for the Cr^{3+}- doped $La_3GaGe_5O_{16}$ phosphors.

Fig. 5 PL spectra for the $La_3Ga_{1-x}Ge_5O_{16}$:$x$$Cr^{3+}$ (x = 0.01, 0.03, 0.05, 0.08, 0.10 and 0.15) phosphors, and the inset shows Cr^{3+} concentration dependence of PL intensity.

Fig. 6 The fitting curve of log(I/x) vs. log(x) in $La_3Ga_{1-x}Ge_5O_{16}$:$x$$Cr^{3+}$ phosphors.

Fig. 7 Room temperature decay curves of $La_3Ga_{1-x}Ge_5O_{16}$:$x$$Cr^{3+}$phosphors with different Cr^{3+} contents x = 0.01, 0.03, 0.05, 0.08 and 0.15.

Fig. 8 Temperature-dependent PL spectra of typical $La_3Ga_{0.97}Ge_5O_{16}$:0.03Cr^{3+}. The inset shows the variation of the temperature dependent relative emission intensities for $La_3Ga_{1-x}Ge_5O_{16}$:$x$$Cr^{3+}$ (x = 0.01, 0.03 and 0.15).

Fig. 9 A ln[(I_0/I_T)-1] vs. 1/K_BT fitting plot and the corresponding activation energy

derived from the thermal quenching data of $La_3Ga_{1-x}Ge_5O_{16}:xCr^{3+}$ (x = 0.01, 0.03 and 0.15).

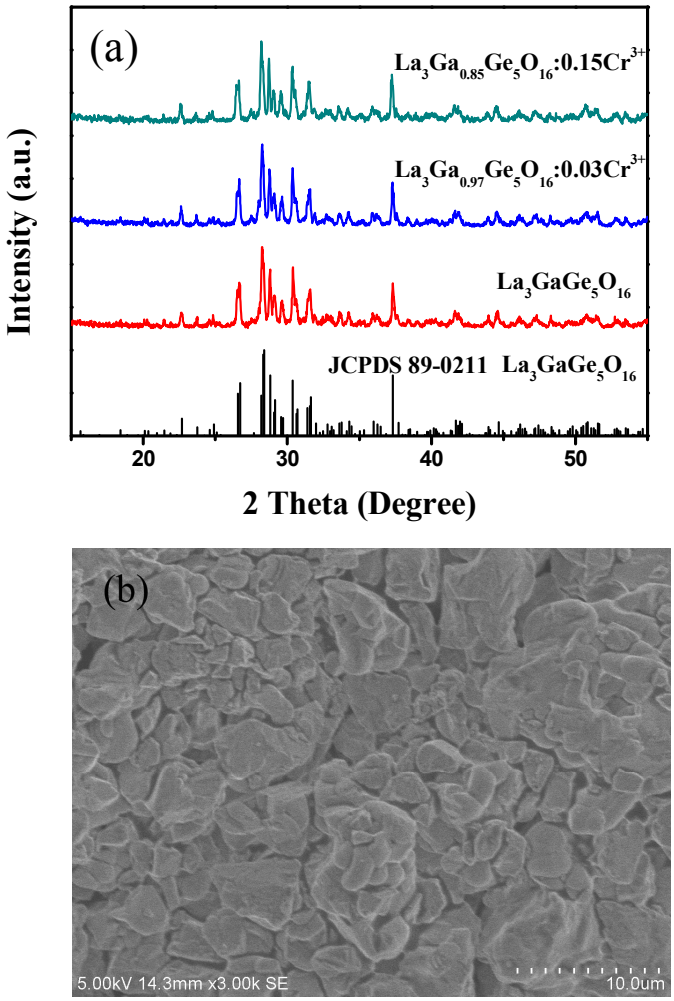

Fig. 1 (a) XRD patterns of as-prepared $La_3GaGe_5O_{16}$, $La_3Ga_{0.97}Ge_5O_{16}$:0.03Cr^{3+}, and $La_3Ga_{0.85}Ge_5O_{16}$:0.15Cr^{3+} phosphors, the standard data for $La_3GaGe_5O_{16}$ (JCPDS card no. 89-0211) is shown as a reference. (b) SEM image of the selected $La_3Ga_{0.97}Ge_5O_{16}$:0.03Cr^{3+} phosphor.

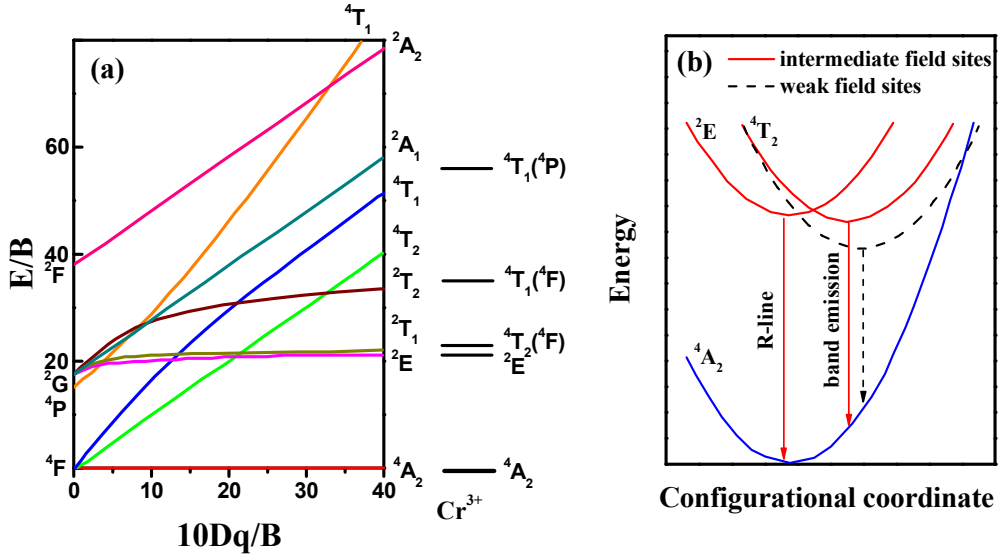

Fig. 2 (a) Tunabe-sugnano diagram for Cr^{3+} in $La_3Ga_{0.97}Ge_5O_{16}$. (b) Mechanistic configurational coordinate diagram illustrating different emission channels. The solid and dashed arrows represent the emissions from the Cr^{3+} ions located in the intermediate and weak field sites, respectively.

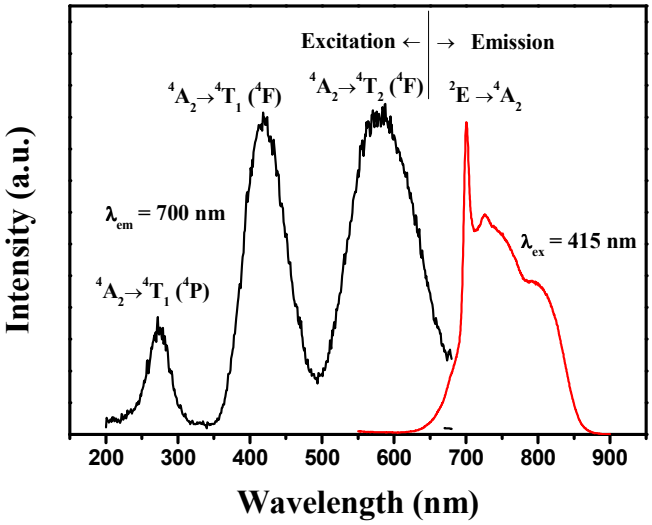

Fig. 3 Normalized excitation and emission spectra of $La_3Ga_{0.97}Ge_5O_{16}$:0.03Cr^{3+} phosphor at room temperature.

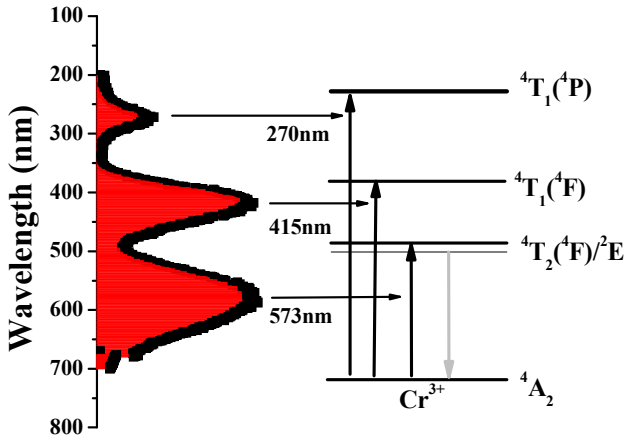

Fig. 4 Schematic energy levels of Cr^{3+}, the corresponding excitation spectrum and electron transitions for the Cr^{3+}- doped $La_3GaGe_5O_{16}$ phosphors.

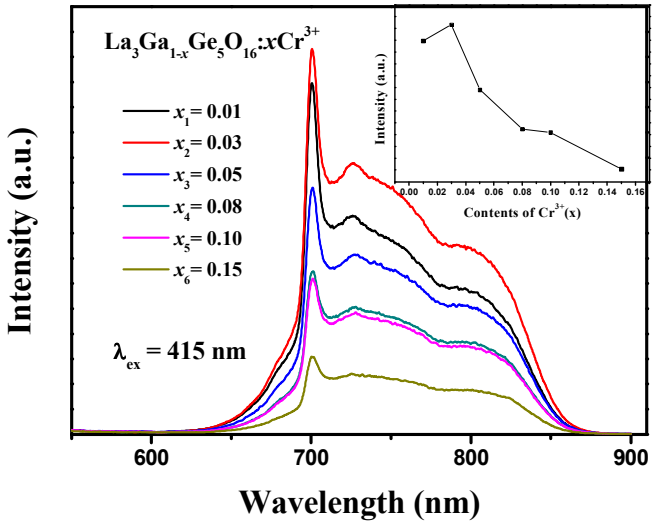

Fig. 5 PL spectra for the phosphors $La_3Ga_{1-x}Ge_5O_{16}:xCr^{3+}$ (x = 0.01, 0.03, 0.05, 0.08, 0.10 and 0.15), and the inset shows Cr^{3+} concentration dependence of PL intensity.

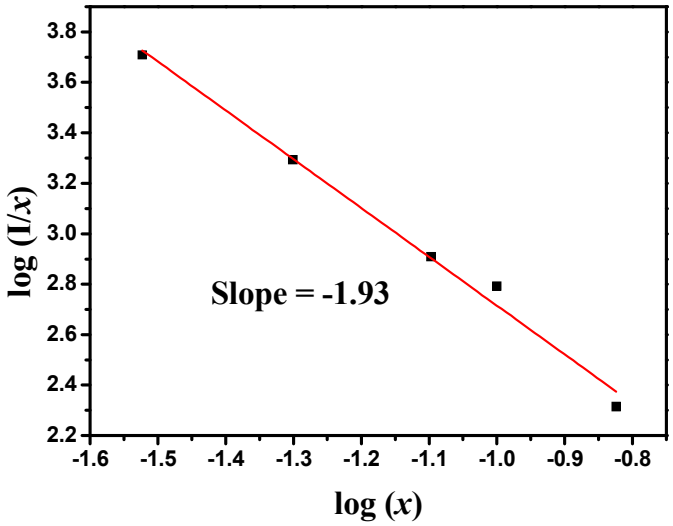

Fig. 6 The fitting curve of log(I/x) vs. log(x) in $La_3Ga_{1-x}Ge_5O_{16}:xCr^{3+}$ phosphors.

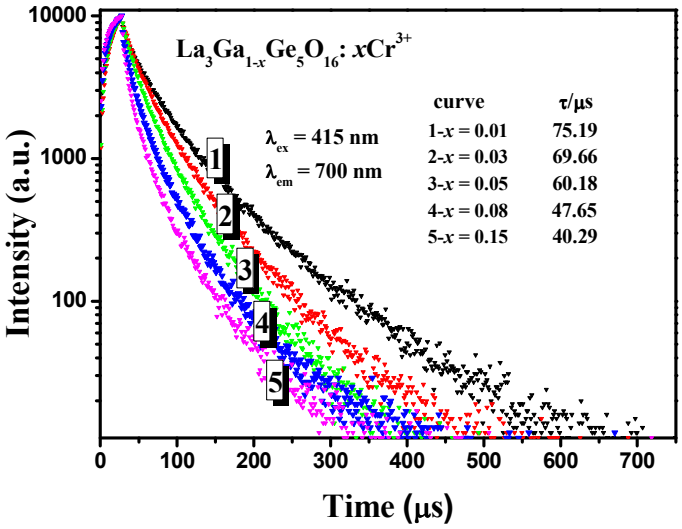

Fig. 7 Room temperature decay curves of $La_3Ga_{1-x}Ge_5O_{16}$:xCr^{3+}phosphors with different Cr^{3+} contents x = 0.01, 0.03, 0.05, 0.08 and 0.15.

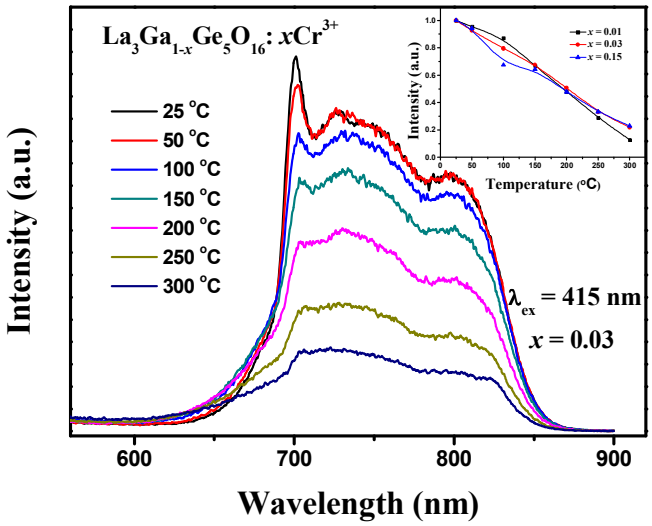

Fig. 8 Temperature-dependent PL spectra of typical $La_3Ga_{0.97}Ge_5O_{16}$:0.03Cr^{3+}. The inset shows the variation of the temperature dependent relative emission intensities for $La_3Ga_{1-x}Ge_5O_{16}$:xCr^{3+} (x = 0.01, 0.03 and 0.15).

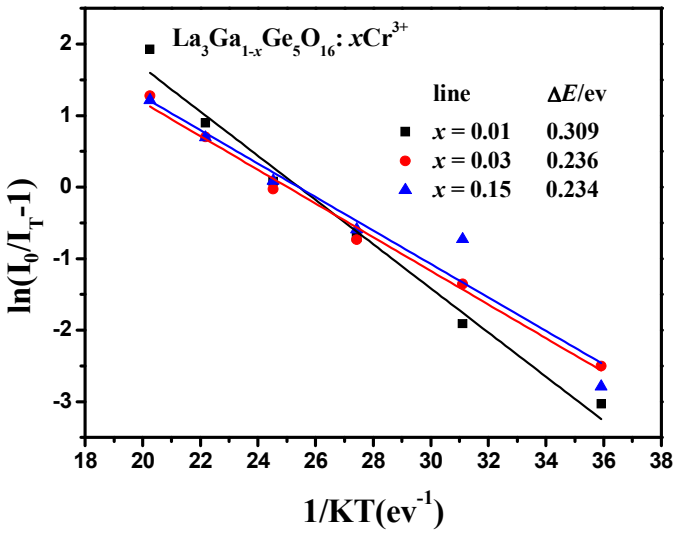

Fig. 9 A $\ln[(I_0/I_T)-1]$ vs. $1/K_BT$ fitting plot and the corresponding activation energy derived from the thermal quenching data of $La_3Ga_{1-x}Ge_5O_{16}:xCr^{3+}$ (x = 0.01, 0.03 and 0.15).